THE JOURNAL OF PHYSICAL CHEMISTRY LETTERS
A JOURNAL OF THE AMERICAN CHEMICAL SOCIETY

pubs.acs.org/JPCL

Letter

Enantioselective Topological Frequency Conversion

Kai Schwennicke and Joel Yuen-Zhou*

Cite This: J. Phys. Chem. Lett. 2022, 13, 2434−2441

Read Online

ACCESS | Metrics & More | Article Recommendations | Supporting Information

ABSTRACT: Two molecules are enantiomers if they are nonsuperimposable mirror images of each other. Electric dipole-allowed cyclic transitions $|1\rangle \rightarrow |2\rangle \rightarrow |3\rangle \rightarrow |1\rangle$ obey the symmetry relation $O^R = -O^S$, where $O^{R,S} = (\mu_{21}^{R,S}E_{21})(\mu_{13}^{R,S}E_{13})(\mu_{32}^{R,S}E_{32})$ and R and S label the two enantiomers. Herein, we generalize the concept of topological frequency conversion to an ensemble of enantiomers. We show that, within a rotating-frame, the pumping power between fields of frequency ω_1 and ω_2 is sensitive to enantiomeric excess, $\mathcal{P}_{2\rightarrow 1} = \hbar[\omega_1\omega_2 C_L^R/(2\pi)](N_R - N_S)$, where N_i is the number of enantiomers i and C_L^R is an enantiomer-dependent Chern number. Connections with chiroptical microwave spectroscopy are made. Our work provides an underexplored and fertile connection between topological physics and molecular chirality.

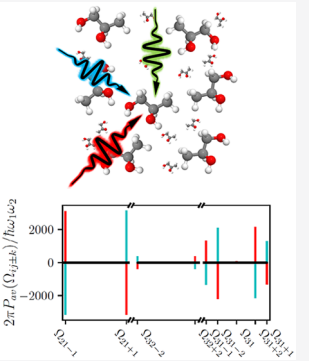

In the mid-19th century, Louis Pasteur discovered that molecules can possess handedness, or chirality, an attribute that influences how they interact with their surroundings.[1] More generally, the two species of a chiral molecule, referred to as enantiomers, are nonsuperimposable mirror images of each other and, while they feature many identical physicochemical properties (up to very small parity violation corrections[2]), they can also exhibit drastically different behavior when exposed to chiral environments or stimuli. Thus, enantioselectivity plays a crucial role in biological activity as well as in the synthesis, purification, and characterization of pharmaceuticals.[3−5] Traditionally, optical rotation and circular dichroism have served as optical tools to obtain enantioselective information; however, these techniques rely on the weak interaction between molecules and the magnetic component of the optical field. A very active effort in chirality research consists of spatially shaping electromagnetic fields[6−8] to enhance these weak interactions. Other techniques that rely solely on electric dipole interactions[9] have been recently advocated. For instance, many efforts are currently invested in photoelectron circular dichroism (PECD).[10−13] Yet, others focus on nonlinear optical signals that depend on the sign of the electric fields with which the molecules interact,[14,15] including photoexcitation circular dichroism,[16] the use of synthetic chiral fields,[17−20] and microwave three-wave mixing.[21−25] More precisely, the latter technique can be understood through cyclic three-level models[26−32] where the product of three light−matter couplings [hereafter termed the Král−Shapiro (KS) product] differs by a phase of π between the two enantiomers. This remarkable symmetry has been exploited to propose cyclic population-transfer schemes[26,32] or the use of cross-polarized terahertz pulses[33] to prepare the enantiomers in different energy configurations or orientations for separation. This symmetry has also been utilized to suggest an enantioselective generalization of the Stern−Gerlach[34] or spin Hall[35] experiments, where spatial separation of enantiomers, rather than spins, is achieved using artificial gauge fields.[36−38] The analogy between enantiomer and spin labels is intriguing and surprisingly underexplored and serves as the motivation of our present work. More specifically, we wish to demonstrate an enantioselective analogue to the quantum spin Hall effect (QSHE).[39]

On the other hand, since the pioneering work of Thouless, Kohmoto, Nightingale, and den Nijs in relation to the quantum Hall effect (QHE),[40] notions of symmetry-protected topological phases (SPTPs) have been at the heart of condensed matter research and have only been exacerbated in the past 15 years with the discovery of topological insulators.[41] These notions guarantee that certain response properties of so-called topologically nontrivial systems are largely independent of material specification, instead depending only on products of universal constants and integer quantities known as topological invariants. The discrete nature of these properties implies that they are robust against material imperfections, thus making them attractive for metrology, among other applications. While topological protection was originally identified in translationally invariant 2D systems, its scope has been enlarged through the use of Floquet engineering in systems of different dimensionality[42−45] and the consideration of the 2D phase space of 1D

Received: December 23, 2021
Accepted: March 2, 2022
Published: March 8, 2022

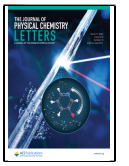

systems.[46,47] Of particular interest is an elegant construction due to Martin, Refael, and Halperin[48] called topological frequency conversion (TFC), where quantized "current" is observed. In this Letter, we design a novel spectroscopic scheme that generalizes TFC to the microwave spectroscopy of an ensemble of chiral molecules. The very first link between chiroptical spectroscopy and topology was suggested recently in work by Ordoñez and Smirnova[49] within the context of PECD. These authors showed that the propensity field (a pseudoscalar) as a function of ejected photoelectron direction (Berry curvature) can be integrated over all solid angles to yield a quantized enantiosensitive flux which is proportional to a Chern number. Similarly, the authors showed that microwave three-wave mixing signals can be interpreted in terms of an analogous quantity to the propensity field.[9] However, it is not clear from that work if there exists a parameter space upon which integration of the signals lead to topological invariants, so geometric and topological consequences of these nonlinear spectroscopies were not explored. In this Letter, we use TFC to identify time as the missing parameter space and for simplicity restrict our attention to frequency conversion rather than three-wave mixing. The result is a signal that is proportional to enantiomeric excess (EE), with a simple prefactor containing the sign of the KS product. Owing to the topological nature of the signal, it should also serve as a very sensitive detection of EE. As far as we are aware, our work provides the first connection between topological physics, chiroptical spectroscopy, and nonlinear spectroscopy and anticipates a fertile ground for further exploration.

Following the principles of enantioselective microwave three wave-mixing,[50,51] we treat the enantiomers as asymmetric tops whose Hamiltonian is

$$H_0 = AJ_a^2 + BJ_b^2 + CJ_c^2 \tag{1}$$

where J_a, J_b, and J_c are the angular momentum operators with respect to the principal axes $\hat{\mathbf{a}}$, $\hat{\mathbf{b}}$, and $\hat{\mathbf{c}}$, respectively, and $A > B > C$ are the corresponding rotational constants. The eigenstates are labeled as $|J, \tau, M\rangle$, where $J = 0, 1, 2, \ldots$ is the rotational quantum number; $M = -J, -J+1, -J+2, \ldots, J$ is the quantum number that characterize the projection of the total angular momentum along the z-laboratory-fixed axis; and τ serves as the quantum number to differentiate between states with the same J and M. We consider the following low angular momentum eigenstates of eq 1 with a rotational quantum number of $J = 0$ or $J = 1$

$$\begin{aligned} &|0, \tau = 1, 0\rangle \\ &|1, \tau = 2, M\rangle \\ &|1, \tau = 3, M\rangle \end{aligned} \tag{2}$$

where $M = -1, 0, 1$[52] (see Supporting Information section 1, SI-1). The ground state $|0, \tau = 1, 0\rangle$, with energy $\hbar\epsilon_1$, and the excited states $|1, \tau = 2, M\rangle$ and $|1, \tau = 3, M\rangle$, with energies $\hbar\epsilon_2$ and $\hbar\epsilon_3$, respectively, are coupled to each other using a set of three orthogonally polarized time-dependent electric fields

$$\begin{aligned} \mathbb{E}_{21}(t) &= \mathcal{E}_{21}(t)\sin(\Omega_{21}t)\hat{\boldsymbol{y}} \\ \mathbb{E}_{32}(t) &= \mathcal{E}_{32}(t)\cos(\Omega_{32}t)\hat{\boldsymbol{x}} \\ \mathbb{E}_{31}(t) &= \mathcal{E}_{31}(t)\cos(\Omega_{31}t)\hat{\boldsymbol{z}} \end{aligned} \tag{3}$$

where $\hat{\boldsymbol{x}}$, $\hat{\boldsymbol{y}}$, and $\hat{\boldsymbol{z}}$ denote the three laboratory-fixed axes; the frequencies $\Omega_{21} = \epsilon_2 - \epsilon_1 - \delta$, $\Omega_{32} = \epsilon_3 - \epsilon_2 - \delta$, and $\Omega_{31} = \epsilon_3 - \epsilon_1 - 2\delta$ are slightly detuned from the system's natural frequencies; and the field amplitudes $\mathcal{E}_{21}(t)$, $\mathcal{E}_{32}(t)$, and $\mathcal{E}_{31}(t)$ are slowly modulated. Note from the selection rules for electric dipole interactions[51] that $\Delta M = 0$ for the z polarized field and $\Delta M = \pm 1$ for the x and y polarized field (see Figure 1). Ignoring all states that are not coupled through the driving electric fields, and assuming that $|\mu^{R,S}_{i,M';j,M}\mathcal{E}_{ij}(t)|/2 \ll \hbar\Omega_{ij}$, the Hamiltonian for the laser dressed R- and S-enantiomer, after making the rotating wave approximation, is

$$\begin{aligned} H^{R,S}(t) = &\sum_{i=1,3} \hbar\epsilon_i |i, 0\rangle\langle i, 0| + \hbar\epsilon_2 \sum_{M=\pm1} |2, M\rangle\langle 2, M| \\ &- \mathcal{E}_{21}(t) \sum_{M=\pm1} \left(\frac{i\mu^{R,S}_{2,M;1,0} e^{-i\Omega_{21}t}}{2} |2, M\rangle\langle 1, 0| + \text{h.c.} \right) \\ &- \mathcal{E}_{32}(t) \sum_{M=\pm1} \left(\frac{\mu^{R,S}_{3,0;2,M} e^{-i\Omega_{32}t}}{2} |3, 0\rangle\langle 2, M| + \text{h.c.} \right) \\ &- \mathcal{E}_{31}(t) \left(\frac{\mu^{R,S}_{3,0;1,0} e^{-i\Omega_{31}t}}{2} |3, 0\rangle\langle 1, 0| + \text{h.c.} \right) \end{aligned} \tag{4}$$

where for simplicity we have introduced the notation $|1, 0\rangle \equiv |0, \tau = 1, 0\rangle$, $|2, M\rangle \equiv |1, \tau = 2, M\rangle$, and $|3, 0\rangle \equiv |1, \tau = 3, 0\rangle$. In eq 4, $\mu^{R,S}_{i,M';j,M}$ is the component of the transition-dipole moment for the $|j, M\rangle \rightarrow |i, M'\rangle$ transition that is projected along the polarization axis of $\mathbb{E}_{ij}(t)$. Following the procedure of refs 50 and 51, the values of $\mu^{R,S}_{i,M';j,M}$ are

$$\begin{aligned} \mu^{R,S}_{2,\pm1;1,0} &= -\frac{i\mu^{R,S}_b}{\sqrt{6}} \\ \mu^{R,S}_{3,0;2,\pm1} &= \frac{\mu^{R,S}_a}{2\sqrt{2}} \\ \mu^{R,S}_{3,0;1,0} &= -\frac{i\mu^{R,S}_c}{\sqrt{3}} \end{aligned} \tag{5}$$

where $\mu^{R,S}_a$, $\mu^{R,S}_b$, $\mu^{R,S}_c$ are the components of the dipole moment along the principal molecular axes. These components are real valued and $|\mu^R_a| = |\mu^S_b|$. Note that for the chosen polarizations for the three electric fields (see eq 3) and studied energy levels, $\mu^{R,S}_{i,M';j,M}$ does not depend on the quantum number M. The associated time-dependent wave function for the R- and S-enantiomer of the system is $|\psi^{R,S}(t)\rangle$.

Next, we consider the rotating frame

$$\begin{aligned} U(t) = &e^{-i(\epsilon_2-\Omega_{21})t}|1, 0\rangle\langle 1, 0| + \sum_{M=\pm1} e^{-i\epsilon_2 t}|2, M\rangle\langle 2, M| \\ &+ e^{-i(\epsilon_2+\Omega_{32})t}|3, 0\rangle\langle 3, 0| \end{aligned} \tag{6}$$

such that $|\psi^{R,S}(t)\rangle = U(t)|\tilde{\psi}^{R,S}(t)\rangle$, in order to remove the central frequencies Ω_{ij}. In this frame, $i\hbar\partial_t|\tilde{\psi}^{R,S}(t)\rangle = \mathcal{H}^{R,S}(t)|\tilde{\psi}^{R,S}(t)\rangle$, with the effective Hamiltonian

https://doi.org/10.1021/acs.jpclett.1c04161
J. Phys. Chem. Lett. 2022, 13, 2434−2441

$$\mathcal{H}^{R,S}(t) = \frac{1}{2}\begin{pmatrix} -2\hbar\delta & -\frac{\mu_b^{R,S}}{\sqrt{6}}\mathcal{E}_{21}(t) & -\frac{\mu_b^{R,S}}{\sqrt{6}}\mathcal{E}_{21}(t) & -\frac{i\mu_c^{R,S}}{\sqrt{3}}\mathcal{E}_{31}(t) \\ -\frac{\mu_b^{R,S}}{\sqrt{6}}\mathcal{E}_{21}(t) & 0 & 0 & -\frac{\mu_a^{R,S}}{2\sqrt{2}}\mathcal{E}_{32}(t) \\ -\frac{\mu_b^{R,S}}{\sqrt{6}}\mathcal{E}_{21}(t) & 0 & 0 & -\frac{\mu_a^{R,S}}{2\sqrt{2}}\mathcal{E}_{32}(t) \\ \frac{i\mu_c^{R,S}}{\sqrt{3}}\mathcal{E}_{31}(t) & -\frac{\mu_a^{R,S}}{2\sqrt{2}}\mathcal{E}_{32}(t) & -\frac{\mu_a^{R,S}}{2\sqrt{2}}\mathcal{E}_{32}(t) & 2\hbar\delta \end{pmatrix} \tag{7}$$

After a change of basis (see SI-2), we arrive at the following effective Hamiltonian:

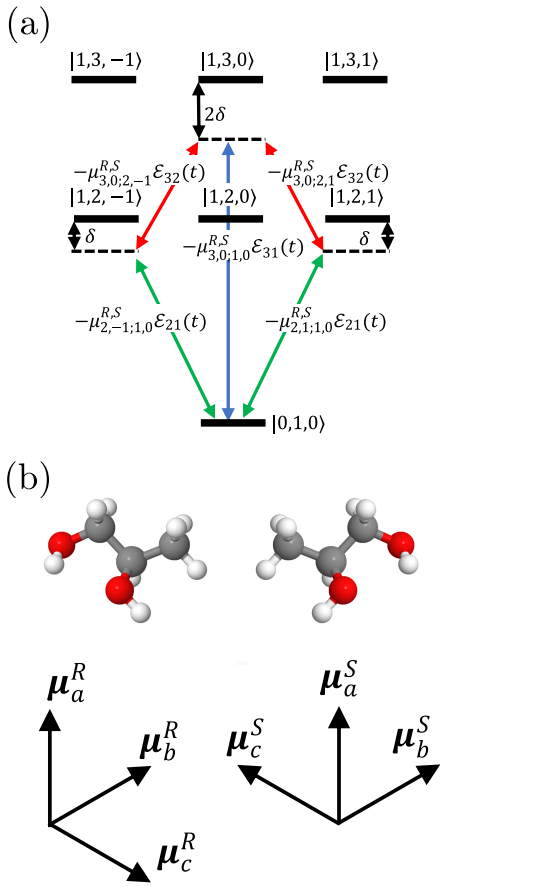

Figure 1. The model. (a) Cyclic three-level transitions for an asymmetric top, such as enantiomers. Three near-resonant, linear polarized lasers with modulated field amplitudes $\mathcal{E}_{ij}(t)$ interact with these transitions. (b) Principal axes components of the dipole moments for the *R*- and *S*-1,2-propanediol enantiomers. Note that $(\boldsymbol{\mu}_a^R\cdot\hat{\boldsymbol{a}})(\boldsymbol{\mu}_b^R\cdot\hat{\boldsymbol{b}})(\boldsymbol{\mu}_c^R\cdot\hat{\boldsymbol{c}}) = -(\boldsymbol{\mu}_a^S\cdot\hat{\boldsymbol{a}})(\boldsymbol{\mu}_b^S\cdot\hat{\boldsymbol{b}})(\boldsymbol{\mu}_c^S\cdot\hat{\boldsymbol{c}})$.

$$\mathcal{H}^{R,S}(t) = -\frac{\mu_b^{R,S}\mathcal{E}_{21}(t)}{2\sqrt{3}\hbar}L_x - \frac{\mu_a^{R,S}\mathcal{E}_{32}(t)}{4\hbar}L_y + \frac{\mu_c^{R,S}\mathcal{E}_{31}(t)}{2\sqrt{3}\hbar} L_z - \frac{\delta}{2\hbar}(L_+^2 + L_-^2) \tag{8}$$

where $L_x = \frac{\hbar}{\sqrt{2}}\begin{pmatrix}0&1&0\\1&0&1\\0&1&0\end{pmatrix}$, $L_y = \frac{\hbar}{\sqrt{2}}\begin{pmatrix}0&-i&0\\i&0&-i\\0&i&0\end{pmatrix}$, and $L_z = \hbar\begin{pmatrix}1&0&0\\0&0&0\\0&0&-1\end{pmatrix}$ are the angular momentum operators for a spin-1 particle and $L_+ = \sqrt{2}\hbar\begin{pmatrix}0&1&0\\0&0&1\\0&0&0\end{pmatrix}$ and $L_- = \sqrt{2}\hbar\begin{pmatrix}0&0&0\\1&0&0\\0&1&0\end{pmatrix}$ are the corresponding ladder operators. We use the form of the effective Hamiltonian in eq 8 to calculate the toplogy of the system. Hereafter, we will assume that the slowly modulated electric field amplitudes are

$$\begin{aligned}\mathcal{E}_{21}(t) &= E_{21}\sin(\omega_1 t)\\ \mathcal{E}_{32}(t) &= E_{32}\sin(\omega_2 t)\\ \mathcal{E}_{31}(t) &= E_{31}[m - \cos(\omega_1 t) - \cos(\omega_2 t)]\end{aligned} \tag{9}$$

where ω_1 and ω_2 are two modulation frequencies and m is a scalar that characterizes a nonmodulated component of the electric field. These functional forms are inspired from the TFC scheme reported in ref 53.

For completeness, we briefly rederive the TFC formalism using adiabatic perturbation theory (the original paper does so within Floquet theory[48]). In the rotating frame, the rate of the system's energy absorption for the enantiomers is given by $\partial_t E^{R,S}(t) = \langle\tilde{\psi}^{R,S}(t)|\partial_t\mathcal{H}^{R,S}(t)|\tilde{\psi}^{R,S}(t)\rangle$. In the long time limit, $t\to\infty$, the time-averaged energy-absorption rate, or average power, is

$$\mathcal{P}_{\mathrm{av}}^{R,S} = \lim_{t\to\infty}\frac{1}{t}\int_0^t \mathrm{d}t'\partial_{t'}E^{R,S}(t') = \sum_{\omega_i}\mathcal{P}_{\mathrm{av}}^{R,S}(\omega_i) \tag{10a}$$

$$\mathcal{P}_{\mathrm{av}}^{R,S}(\omega_i) = \lim_{t\to\infty}\frac{1}{t}\int_0^t \mathrm{d}t'\omega_i\langle\partial_{\omega_i t'}\mathcal{H}^{R,S}(t')\rangle \tag{10b}$$

where $\mathcal{P}_{\mathrm{av}}^{R,S}(\omega_i)$ is the average power at the modulation frequency ω_i.

Let $|\epsilon_l^{R,S}(t)\rangle$ denote the l-th adiabatic state of $\mathcal{H}^{R,S}(t)$, where $\mathcal{H}^{R,S}(t)|\epsilon_l^{R,S}(t)\rangle = \epsilon_l^{R,S}(t)|\epsilon_l^{R,S}(t)\rangle$ (Figure 2). If ω_1 and ω_2 are incommensurate, i.e., ω_1/ω_2 is irrational, $\mathcal{H}^{R,S}(t)$ is not periodic. However, if we write $\mathcal{H}^{R,S}(t) = \mathcal{H}^{R,S}(\boldsymbol{\theta}) = \mathcal{H}^{R,S}(\theta_1, \theta_2)$with $\theta_i = \omega_i t \pmod{2\pi}$, we notice that $\mathcal{H}^{R,S}(\boldsymbol{\theta})$ is quasiperiodic, $\mathcal{H}^{R,S}(\theta_1 + 2\pi, \theta_2) = \mathcal{H}^{R,S}(\theta_1, \theta_2 + 2\pi) = \mathcal{H}^{R,S}(\theta_1, \theta_2)$, and the domain of $\mathcal{H}^{R,S}(\theta_1, \theta_2)$ is a two-dimensional torus $\mathbb{T} = [0, 2\pi)\otimes[0, 2\pi)$. Near the adiabatic limit where ω_1 and ω_2 are much smaller than the instantaneous energy gap of $\mathcal{H}^{R,S}(t)$, and if the system is initiated in the l-th adiabatic state, i.e., $|\tilde{\psi}^{R,S}(0)\rangle = |\epsilon_l^{R,S}(0)\rangle$, the expected quantities $\langle\partial_{\omega_1 t}\mathcal{H}^{R,S}(t)\rangle$ and $\langle\partial_{\omega_2 t}\mathcal{H}^{R,S}(t)\rangle$ for $|\tilde{\psi}^{R,S}(t)\rangle$, to first order in ω_1 and ω_2 are

$$\langle\partial_{\omega_1 t}\mathcal{H}^{R,S}(t)\rangle = \langle\partial_{\theta_1}\mathcal{H}^{R,S}(\boldsymbol{\theta})\rangle = \partial_{\theta_1}\epsilon_l^{R,S}(\boldsymbol{\theta}) - \hbar\omega_2 F_l^{R,S}(\boldsymbol{\theta}) \tag{11a}$$

$$\langle\partial_{\omega_2 t}\mathcal{H}^{R,S}(t)\rangle = \langle\partial_{\theta_2}\mathcal{H}^{R,S}(\boldsymbol{\theta})\rangle = \partial_{\theta_2}\epsilon_l^{R,S}(\boldsymbol{\theta}) + \hbar\omega_1 F_l^{R,S}(\boldsymbol{\theta}) \tag{11b}$$

where $F_l^{R,S}(\boldsymbol{\theta}) = i\langle\partial_{\theta_1}\epsilon_l^{R,S}(\boldsymbol{\theta})|\partial_{\theta_2}\epsilon_l^{R,S}(\boldsymbol{\theta})\rangle + \mathrm{h.c.}$ is the Berry curvature of the l-th adiabatic state (see SI-3).

https://doi.org/10.1021/acs.jpclett.1c04161
J. Phys. Chem. Lett. 2022, 13, 2434−2441

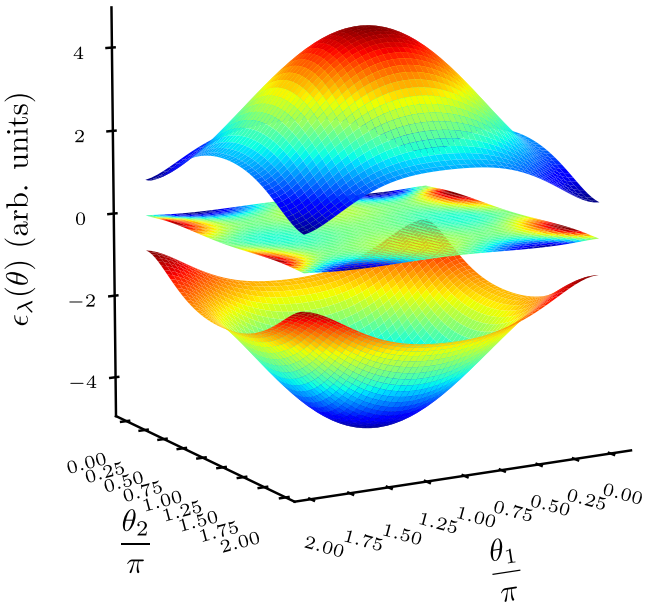

Figure 2. Example adiabatic bands giving rise to enantioselective TFC. The color gradient is a visual aid for the band dispersion.

According to the mean-value theorem for incommensurate ω_1 and ω_2,[54] the linear flow of $\boldsymbol{\theta}$ covers the torus densely for long enough times. Thus, the time average of $F_l^{R,S}(t)$ is the same as the average of $F_l^{R,S}(\boldsymbol{\theta})$ over the entire torus $\mathbb{T}$:

$$\lim_{t\to\infty}\frac{1}{t}\int_0^t \mathrm{d}t' F_l^{R,S}(t') = \frac{1}{4\pi^2}\int_{\mathbb{T}} \mathrm{d}\boldsymbol{\theta} F_l^{R,S}(\boldsymbol{\theta}) \tag{12}$$

From a practical standpoint, $t\to\infty$ means $t > p\frac{2\pi}{\omega_1} = q\frac{2\pi}{\omega_2}$, where $\frac{\omega_1}{\omega_2}\approx\frac{p}{q}$ for $p, q\in\mathbb{Z}^+$. Substituting eqs 11a and 11b into eq 10b gives rise to the average power lost by the fields at ω_1 and ω_2 when the system is initiated in the l-th adiabatic state, $\mathcal{P}_{\mathrm{av}}^{R,S}(\omega_1) = -\mathcal{P}_{\mathrm{av}}^{R,S}(\omega_2) = -\frac{\hbar\omega_1\omega_2 C_l^{R,S}}{2\pi}$. Here the average of $\partial_{\theta_i}\epsilon_l^{R,S}(\boldsymbol{\theta})$ is zero because $\epsilon_l^{R,S}(\boldsymbol{\theta})$ is quasiperiodic in $\boldsymbol{\theta}$, and $C_l^{R,S} = \frac{1}{2\pi}\int_{\mathbb{T}}\mathrm{d}\boldsymbol{\theta}F_l^{R,S}(\boldsymbol{\theta})$ is the Chern number of the l-th adiabatic state for the corresponding enantiomer. Thus, the enantiomer-dependent average energy-pumping rate between the two modulation fields $\mathcal{P}_{2\to1}^{R,S} = [\mathcal{P}_{\mathrm{av}}^{R,S}(\omega_2) - \mathcal{P}_{\mathrm{av}}^{R,S}(\omega_1)]/2$ is quantized

$$\mathcal{P}_{2\to1}^{R,S} = \frac{\hbar\omega_1\omega_2 C_l^{R,S}}{2\pi} \tag{13}$$

or in other words, after one period of the ω_2 modulation, $C_l^{R,S}$ photons with frequency ω_1 are produced. The photons produced are in the same spatial modes as the incoming electric fields. The very off-resonant nature of this process guarantees that the molecule does not retain energy and the energy-transfer process occurs only between the fields.

For $\delta = 0$, $\mathcal{H}^{R,S}(\boldsymbol{\theta})$ (see eq 8) resembles half of the Bernevig−Hughes−Zhang Hamiltonian,[55] except that the Pauli matrices are replaced with the spin-1 angular momentum operators. As expected, $\mathcal{H}^{R,S}(\boldsymbol{\theta})$ is topologically nontrivial for $|m| < 2$, where the Chern numbers for the upper (U) and lower (L) adiabatic states remarkably acquire the value

$$C_U^{R,S} = 2\mathrm{sgn}(m)\mathrm{sgn}(O^{R,S}) = -C_L^{R,S} \tag{14}$$

and that for the middle (M) adiabatic state $C_M = 0$ (for an analytical proof, see SI-4). $O^{R,S} = (\mu_b^{R,S}E_{12})(\mu_a^{R,S}E_{23})(\mu_c^{R,S}E_{31})$ is the KS product which obeys the enantioselective symmetry relation $O^R = -O^S$, because $\mu_a^R\mu_b^R\mu_c^R = -\mu_a^S\mu_b^S\mu_c^S$, and we have assumed that $E_{ij} = E_{ji}$. Therefore, $C_L^R = -C_L^S$, and the TFC for the two enantiomers initiated in the lower (upper) adiabatic state at $t = 0$ is expected to have the same magnitude but opposite sign, i.e., $\mathcal{P}_{2\to1}^R = -\mathcal{P}_{2\to1}^S$. This results begs us to consider the fruitful analogy between enantiomer label and spin degrees of freedom. Just like in the QSHE, where the transverse conductivity for opposite spins bears opposite signs, so does the TFC for opposite enantiomers. Equation 14 is the central result of this Letter and relates a fundamental topological invariant from chiroptical spectroscopy ($\mathrm{sgn}\, O = \pm1$) with the notions of SPTPs. Figure 3 shows the computed value of C_L^R for different values of m when $\delta\neq0$.

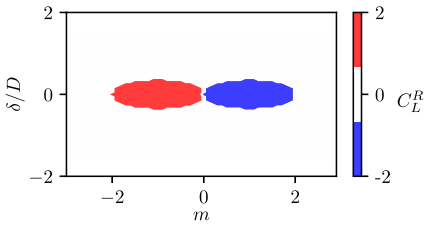

Figure 3. Topological phase diagram. The value of C_L^R is calculated taking the magnitudes of the light−matter couplings to be equal, i.e., $|\mu_{2,M';1M}^R E_{21}| = |\mu_{3,M';2,M}^R E_{32}| = |\mu_{3,M';1,M}^R E_{31}| = \hbar D$, while the laser-driving parameters m and δ are varied. We obtain $C_L^R = -2\mathrm{sgn}(m)\mathrm{sgn}(O^R)$ at the vicinity of $\delta = 0$, where $O^R = -O^S$ is the Král−Shapiro product, which is enantioselective.

By analogy with eq 10a, we can compute the enantiomer-dependent average power absorbed in the original frame as $P_{\mathrm{av}}^{R,S}(\Omega) = \lim_{t\to\infty}\frac{1}{t}\int_0^t \mathrm{d}t'\Omega\langle\partial_{\Omega t'}H^{R,S}(t')\rangle$, obtaining

$$\frac{\mathcal{P}_{\mathrm{av}}^{R,S}(\omega_1)}{\hbar\omega_1} = \frac{P_{\mathrm{av}}^{R,S}(\Omega_{21+1})}{\hbar\Omega_{21+1}} - \frac{P_{\mathrm{av}}^{R,S}(\Omega_{21-1})}{\hbar\Omega_{21-1}} + \frac{P_{\mathrm{av}}^{R,S}(\Omega_{31+1})}{\hbar\Omega_{31+1}} - \frac{P_{\mathrm{av}}^{R,S}(\Omega_{31-1})}{\hbar\Omega_{31-1}} \tag{15a}$$

$$\frac{\mathcal{P}_{\mathrm{av}}^{R,S}(\omega_2)}{\hbar\omega_1} = \frac{P_{\mathrm{av}}^{R,S}(\Omega_{32+2})}{\hbar\Omega_{32+2}} - \frac{P_{\mathrm{av}}^{R,S}(\Omega_{32-2})}{\hbar\Omega_{32-2}} + \frac{P_{\mathrm{av}}^{R,S}(\Omega_{31+2})}{\hbar\Omega_{31+2}} - \frac{P_{\mathrm{av}}^{R,S}(\Omega_{31-2})}{\hbar\Omega_{31-2}} \tag{15b}$$

where $\Omega_{ij\pm1,2} = \Omega_{ij}\pm\omega_{1,2}$. Thus, the quantization due to the enantioselective TFC can be extracted from an experimentally detected difference power spectrum of the fields interacting with the molecule. Notice that the topology is preserved for $\delta\neq0$ as long as $\hbar|\delta| < |\mu_{i,M';j,M}^{R,S}E_{ij}|/2$. In general, we expect our scheme to maintain the nontrivial topology with respect to changes in experimental conditions (such as laser spot size or collection efficiency) so long as adiabaticity still holds and the necessary peaks in the power spectrum can be resolved.

https://doi.org/10.1021/acs.jpclett.1c04161
J. Phys. Chem. Lett. 2022, 13, 2434−2441

The dynamics of the system is calculated by numerically integrating the Schrödinger equation in the rotating frame (eq 7), and the power spectrum is obtained by returning to the original frame. In atomic units ($\hbar = 1$), the electric field amplitudes are taken to be $E_{21} = 5\sqrt{3}E_0$, $E_{32} = 6E$, and $E_{31} = \sqrt{3}E_0$, where $E_0 = 4.0 \times 10^{-9}$ a.u., the dipole moment principal axes components are $\mu_a^R = \mu_a^S = 0.47$ a.u., $\mu_b^R = \mu_b^S = 0.75$ a.u., and $\mu_c^R = -\mu_c^S = 0.14$ a.u., and the molecular transition energies are $\epsilon_2 - \epsilon_1 = 4.4 \times 10^{-8}$ a.u. and $\epsilon_3 - \epsilon_1 = 4.7 \times 10^{-8}$ a.u. The dipole moment components and molecular energies are extracted from a microwave three-wave-mixing model for *R*- and *S*-1,2-propanediol.[21] Using these parameters, it is true that $|\mu^{R,S}_{i,M';j,M}E_{ij}|/2 \ll \hbar\Omega_{ij}$, so the rotating wave approximation holds. The slow incommensurate modulation frequencies and laser detuning are taken to be $\omega_1 = \omega_2/\phi = \delta = 1 \times 10^{-11}$ a.u., where we take $\phi = \frac{\sqrt{5}-1}{2}$ as in ref 48, satisfying the perturbative condition $\hbar|\delta|, \hbar\omega_1, \hbar\omega_2 \ll |\mu^{R,S}_{i,M;j,M'}\cdot E_{ij}|/2$. Setting $m = 1.4$, the system is in the topologically nontrivial regime.

To obtain the desired enantioselective TFC, both enantiomers need to be prepared in the lowest adiabatic bands in the rotating frame at $t = 0$. Suppose that before fields are turned on ($\mu^{R,S}_{i,M';j,M}\mathcal{E}_{ij}(t) \to 0$ as $t \to -\infty$), the molecules start in the ground state $|1, 0\rangle$. Under those circumstances, the eigenstates of eq 7 are the states $|1, 0\rangle$, $|2, M\rangle$, and $|3, 0\rangle$ with eigenenergies $\epsilon^{R,S}_{L,M,U}(-\infty) = -\delta, 0, \delta$, and the state of each molecule is $|\epsilon^{R,S}_L(-\infty)\rangle$. If the electric fields are slowly turned on at a rate ω_r that is much smaller than the instantaneous band gaps $|\epsilon^{R,S}_l(t) - \epsilon^{R,S}_{l'}(t)|$, both enantiomers are prepared in the lower adiabatic state, i.e., $|\epsilon^{R,S}_L(0)\rangle$. Note that the modulating frequencies ω_1 and ω_2 must also be much smaller than $|\epsilon^{R,S}_l(t) - \epsilon^{R,S}_{l'}(t)|$ at all times. Chirped microwave fields for $t < 0$ satisfy this constraint. The adiabatic protocol we choose is $E_{ij} \to E_{ij}\alpha(t)$ and $\omega_{1,2} \to \omega_{1,2}\beta(t)$, where the ramp-up functions slowly vary at the rate $\omega_r = 2 \times 10^{-13}$ a.u. (see Figure 4)

$$\alpha(t) = \begin{cases} 0 & t < -\frac{2\pi}{\omega_r} \\ \frac{1 - \cos\omega_r t}{2} & -\frac{2\pi}{\omega_r} < t < -\frac{\pi}{\omega_r} \\ 1 & -\frac{\pi}{\omega_r} < t \end{cases} \tag{16a}$$

$$\beta(t) = \begin{cases} 0 & t < -\frac{\pi}{\omega_r} \\ \frac{1 + \cos\omega_r t}{2} & -\frac{\pi}{\omega_r} < t < 0 \\ 1 & 0 < t \end{cases} \tag{16b}$$

After a sufficiently long time (we choose $t^* = 2000 \times 2\pi/\omega_2$), the frequency-resolved time-averaged power spectrum $P_{av}(\Omega)$ lost by the fields is numerically calculated considering only $t \geq 0$. This quantity is indeed enantioselective, and using eqs 15a and 15b, each enantiomer Chern number for the lower band

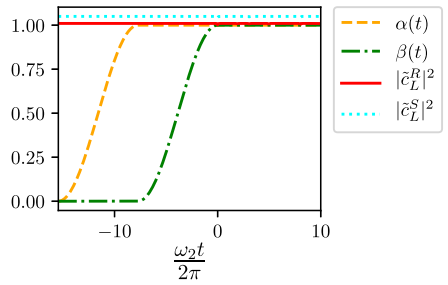

Figure 4. Adiabatic state preparation. Presented are the plots for the functions $\alpha(t)$ and $\beta(t)$. We also feature the populations $|\tilde{c}_L^R|^2$ and $|\tilde{c}_L^S|^2$ (shifted vertically slightly to be visible) of the lower adiabatic state for each enantiomer. As shown, the system is effectively prepared in the lower adiabatic bands for both enantiomers.

$C_L^R = -2 = -C_L^S$ is extracted, revealing the topological nature of this nonlinear optical phenomenon (Figure 5).

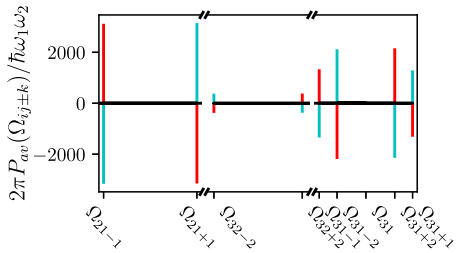

Figure 5. Enantioselective TFC. Plotted is the difference power spectrum for the driving electric field when coupled to a single *R* (red) and *S* (cyan) 1,2-propanediol enantiomers. In terms of intensity, assuming the laser beam waist area is ∼1 cm^2, the change observed is $\sim 10^{-15}$ W·m^{-2} per molecule. This spectrum is enantioselective, and using eqs 15a and 15b, we can see that the frequency conversion in the rotating frame is topological, $\frac{2\pi}{\hbar\omega_1\omega_2}\mathcal{P}^R_{2\to1} = -\frac{2\pi}{\hbar\omega_1\omega_2}\mathcal{P}^S_{1\to2} = -2$.

For an ensemble containing N_R *R*-molecules and N_S *S*-molecules, which are all prepared in the ground state $|1, 0\rangle$, the expected pumping rate is

$$\mathcal{P}_{2\to1} = \frac{\hbar\omega_1\omega_2 C_L^R}{2\pi}(N_R - N_S) \tag{17}$$

which is zero for a racemic mixture but otherwise reveals the EE $|N_R - N_S|$ and chirality $\mathrm{sgn}(N_R - N_S)$. Notice that in line with other nonlinear chiroptical signals that depend on electric but not magnetic dipole contributions,[9] eq 17 contains no background achiral signal, unlike traditional circular dichroism, where both enantiomers have the same electric dipole and magnetic dipole absorption strengths for circularly polarized light.[56]

Let us briefly discuss the limits of enantioselective TFC. First, the line widths of microwave transitions are on the order of 10−100 kHz,[57] which are smaller than the adiabatic state preparation gap $\delta \approx 1$ MHz, as well as the light−matter interactions $|\mu_{ij}E_{ij}|/\hbar \approx 10$ MHz inducing the topological gap, or even the smallest difference in energies in the power spectrum (see Figure 5, $\Omega_{31\pm1} - \Omega_{31\pm2} \approx 1$ MHz). Thus, the described protocol should be resilient to the finite line widths of these transitions. Second, another source of imperfections stems from laser shot noise. Assuming that the laser beam waist area is ∼1 cm^2 and considering the field strength above, the shot noise for a time interval t^* is $\sqrt{N} \sim 10^9$ (where *N* is the expected number of

https://doi.org/10.1021/acs.jpclett.1c04161
J. Phys. Chem. Lett. 2022, 13, 2434−2441

photons produced by the field, see SI-5). From the power spectrum (Figure 5), we find that for the same time interval, the minimal magnitude of the change in the photon number due to the TFC is $\min\left(\left|\frac{P_{av}(\Omega_{ij\pm1,2})t^*}{\hbar\Omega_{ij\pm1,2}}\right|\right) \approx 100 \times |N_R - N_S|$. Therefore, as long as the magnitude of the enantiomer excess $|N_R - N_S|$ is much larger than $\sim 10^7$ molecules, the signal should be detectable above the shot noise. In terms of percentage of the total molecule count $N_R + N_S$, the lower end of the EE detection limit for 1 mL of a 1 μM solution is 10^{-6}%. We conclude with a few comments on the observability of our predictions. First, this study has assumed the ideal limit that the molecules are at 0 K. Under typical experimental conditions for microwave-three wave mixing at 7 K,[21] all three rotational energy levels used in our model are substantially thermally occupied. In this scenario, enantioselective frequency conversion still survives; however, the integer Chern number will be replaced by a thermal average of the Chern numbers C_L^R, C_M^R, C_U^R. Second, the excited-state thermal populations can be bypassed by working in a different energy range, such as the UV−visible one involving electronic transitions and the infrared one involving vibrations;[58,59] the price to pay in the first case is the complication introduced by electron−vibration coupling. These complications will be addressed in future contributions.

In summary, we have presented an enantioselective TFC setup for an ensemble of chiral molecules. Owing to the dependence of the topological invariant on the sign of the KS product (eq 14), which differs by a phase of π for the two enantiomers, the quantized time-averaged energy-pumping rate is of opposite sign for the *R*- and *S*-molecules, just like transverse conductivity is of opposite sign for up and down spins in the QSHE. We show that the computed signal is nonzero for any sample with EE and vanishes for a racemic mixture. An intriguing consequence of eq 13 is that as long as the time scale separations required by the model are fulfilled, the chemical identity of the probed molecules (e.g., through the strengths of the transition dipole moments) in the rotating frame is erased by the signal, leading to a universal nonlinear optical response which acknowledges the enantiomeric excess only. This characteristic is reminiscent of the very accurate determination of the quantum of conductance with a wide range of QHE systems. Thus, from a metrological standpoint, the generality of the enantioselective TFC can be exploited to accurately measure EE by running a linear fit of the pumping rate $\mathcal{P}_{2\to1}$ for a series of experiments where ω_1 (or ω_2) is varied. Furthermore, if one is concerned only with |EE|, a practical asset of the presented methodology is that there is no need to calibrate the signal with an enantiopure sample beforehand. We believe that the removal of calibration counterbalances the complexity of the experimental setup proposed in this Letter.

While concepts of topology have been very productive in the exploration of new condensed matter physics phenomena, most of them are restricted to periodic solids (see refs 60 and 61 for a few molecular exceptions). TFC[44,48] is a powerful tool that opens doors to the application of those concepts to 0D systems such as finite molecular and nonperiodic nanoscale systems. In particular, this work reveals that laser-dressed chiral molecules support SPTPs that are not adiabatically connected to their nonlaser-dressed counterparts. It also provides a fruitful playground to explore further conceptual connections between topological physics and molecular chirality.[49,62]

■ ASSOCIATED CONTENT

Supporting Information

The Supporting Information is available free of charge at https://pubs.acs.org/doi/10.1021/acs.jpclett.1c04161.

Presentation of rotational eigenstates of an asymmetric top; discussion of the change of basis applied to obtain the necessary effective Hamiltonian; review of adiabatic perturbation theory; derivation of the expected laser power in the rotating frame; analytical evaluation of enantioselective Chern number for zero detuning; calculation of expected laser shot noise (PDF)

■ AUTHOR INFORMATION

Corresponding Author

Joel Yuen-Zhou − *Department of Chemistry and Biochemistry, University of California, San Diego, La Jolla, California 92093, United States;* orcid.org/0000-0002-8701-8793; Email: joelyuen@ucsd.edu

Author

Kai Schwennicke − *Department of Chemistry and Biochemistry, University of California, San Diego, La Jolla, California 92093, United States*

Complete contact information is available at: https://pubs.acs.org/10.1021/acs.jpclett.1c04161

Notes

The authors declare no competing financial interest.

■ ACKNOWLEDGMENTS

K.S. and J.Y.-Z. were supported by NSF CAREER CHE 1654732. This work employed computational resources of the Extreme Science and Engineering Discovery Environment (XSEDE), which is supported by National Science Foundation Grant No. ACI-1548562, under allocation No. TG-ASC150024. K.S. acknowledges helpful discussions with Matthew Du, Stephan van den Wildenberg, and Jorge A. Campos-González-Angulo. Both K.S. and J.Y.-Z. acknowledge the help of insightful comments from previous Reviewers.

■ REFERENCES

(1) Pasteur, L. Sur les relations qui peuvent exister entre la forme crystalline, la composition chimique et le sens de la polarization rotatoire. *Ann. Chim. Phys.* **1848**, *24*, 442−459.

(2) Quack, M.; Stohner, J.; Willeke, M. High-resolution spectroscopic studies and theory of parity violation in chiral molecules. *Annu. Rev. Phys. Chem.* **2008**, *59*, 741−769.

(3) Hutt, A. J.; Tan, S. C. Drug chirality and its clinical significance. *Drugs* **1996**, *52*, 1−12.

(4) Kasprzyk-Hordern, B. Pharmacologically active compounds in the environment and their chirality. *Chem. Soc. Rev.* **2010**, *39*, 4466−4503.

(5) Blackmond, D. G. The origin of biological homochirality. *Cold Spring Harbor Perspect. Biol.* **2010**, *2*, a002147.

(6) Tang, Y.; Cohen, A. E. Optical chirality and its interaction with matter. *Phys. Rev. Lett.* **2010**, *104*, 163901.

(7) Poulikakos, L. V.; Thureja, P.; Stollmann, A.; De Leo, E.; Norris, D. J. Chiral light design and detection inspired by optical antenna theory. *Nano Lett.* **2018**, *18*, 4633−4640.

(8) García-Guirado, J.; Svedendahl, M.; Puigdollers, J.; Quidant, R. Enantiomer-selective molecular sensing using racemic nanoplasmonic arrays. *Nano Lett.* **2018**, *18*, 6279−6285.

(9) Ordonez, A. F.; Smirnova, O. Generalized perspective on chiral measurements without magnetic interactions. *Phys. Rev. A* **2018**, *98*, 063428.

(10) Ritchie, B. Theory of the angular distribution of photoelectrons ejected from optically active molecules and molecular negative ions. *Phys. Rev. A* **1976**, *13*, 1411.
(11) Böwering, N.; Lischke, T.; Schmidtke, B.; Müller, N.; Khalil, T.; Heinzmann, U. Asymmetry in photoelectron emission from chiral molecules induced by circularly polarized light. *Phys. Rev. Lett.* **2001**, *86*, 1187.
(12) Lux, C.; Wollenhaupt, M.; Bolze, T.; Liang, Q.; Köhler, J.; Sarpe, C.; Baumert, T. Circular dichroism in the photoelectron angular distributions of camphor and fenchone from multiphoton ionization with femtosecond laser pulses. *Angew. Chem., Int. Ed.* **2012**, *51*, 5001−5005.
(13) Demekhin, P. V.; Artemyev, A. N.; Kastner, A.; Baumert, T. Photoelectron circular dichroism with two overlapping laser pulses of carrier frequencies ω and 2 ω linearly polarized in two mutually orthogonal directions. *Phys. Rev. Lett.* **2018**, *121*, 253201.
(14) Fischer, P.; Wiersma, D. S.; Righini, R.; Champagne, B.; Buckingham, A. D. Three-wave mixing in chiral liquids. *Phys. Rev. Lett.* **2000**, *85*, 4253.
(15) Brumer, P.; Frishman, E.; Shapiro, M. Principles of electric-dipole-allowed optical control of molecular chirality. *Phys. Rev. A* **2001**, *65*, 015401.
(16) Beaulieu, S.; Comby, A.; Descamps, D.; Fabre, B.; Garcia, G. A.; Géneaux, R.; Harvey, A. G.; Légaré, F.; Mašín, Z.; Nahon, L.; et al. Photoexcitation circular dichroism in chiral molecules. *Nat. Phys.* **2018**, *14*, 484−489.
(17) Neufeld, O.; Ayuso, D.; Decleva, P.; Ivanov, M. Y.; Smirnova, O.; Cohen, O. Ultrasensitive chiral spectroscopy by dynamical symmetry breaking in high harmonic generation. *Phys. Rev. X* **2019**, *9*, 031002.
(18) Ayuso, D.; Neufeld, O.; Ordonez, A. F.; Decleva, P.; Lerner, G.; Cohen, O.; Ivanov, M.; Smirnova, O. Synthetic chiral light for efficient control of chiral light−matter interaction. *Nat. Photonics* **2019**, *13*, 866−871.
(19) Neufeld, O.; Even Tzur, M.; Cohen, O. Degree of chirality of electromagnetic fields and maximally chiral light. *Phys. Rev. A* **2020**, *101*, 053831.
(20) Ayuso, D.; Ordonez, A. F.; Decleva, P.; Ivanov, M.; Smirnova, O. Enantio-sensitive unidirectional light bending. *Nat. Commun.* **2021**, *12*, 3951.
(21) Patterson, D.; Schnell, M.; Doyle, J. M. Enantiomer-specific detection of chiral molecules via microwave spectroscopy. *Nature* **2013**, *497*, 475−477.
(22) Patterson, D.; Doyle, J. M. Sensitive chiral analysis via microwave three-wave mixing. *Phys. Rev. Lett.* **2013**, *111*, 023008.
(23) Shubert, V. A.; Schmitz, D.; Patterson, D.; Doyle, J. M.; Schnell, M. Identifying enantiomers in mixtures of chiral molecules with broadband microwave spectroscopy. *Angew. Chem., Int. Ed.* **2014**, *53*, 1152−1155.
(24) Lobsiger, S.; Perez, C.; Evangelisti, L.; Lehmann, K. K.; Pate, B. H. Molecular structure and chirality detection by Fourier transform microwave spectroscopy. *J. Phys. Chem. Lett.* **2015**, *6*, 196−200.
(25) Shubert, V. A.; Schmitz, D.; Pérez, C.; Medcraft, C.; Krin, A.; Domingos, S. R.; Patterson, D.; Schnell, M. Chiral analysis using broadband rotational spectroscopy. *J. Phys. Chem. Lett.* **2016**, *7*, 341−350.
(26) Král, P.; Shapiro, M. Cyclic population transfer in quantum systems with broken symmetry. *Phys. Rev. Lett.* **2001**, *87*, 183002.
(27) Král, P.; Thanopulos, I.; Shapiro, M.; Cohen, D. Two-step enantio-selective optical switch. *Phys. Rev. Lett.* **2003**, *90*, 033001.
(28) Thanopulos, I.; Král, P.; Shapiro, M. Theory of a two-step enantiomeric purification of racemic mixtures by optical means: The D 2 S 2 molecule. *J. Chem. Phys.* **2003**, *119*, 5105−5116.
(29) Li, Y.; Bruder, C. Dynamic method to distinguish between left- and right-handed chiral molecules. *Phys. Rev. A* **2008**, *77*, 015403.
(30) Vitanov, N. V.; Drewsen, M. Highly efficient detection and separation of chiral molecules through shortcuts to adiabaticity. *Phys. Rev. Lett.* **2019**, *122*, 173202.
(31) Kang, Y.-H.; Shi, Z.-C.; Song, J.; Xia, Y. Effective discrimination of chiral molecules in a cavity. *Opt. Lett.* **2020**, *45*, 4952−4955.
(32) Wu, J.-L.; Wang, Y.; Han, J.-X.; Wang, C.; Su, S.-L.; Xia, Y.; Jiang, Y.; Song, J. Two-path interference for enantiomer-selective state transfer of chiral molecules. *Phys. Rev. Appl.* **2020**, *13*, 044021.
(33) Tutunnikov, I.; Xu, L.; Field, R. W.; Nelson, K. A.; Prior, Y.; Averbukh, I. S. Enantioselective orientation of chiral molecules induced by terahertz pulses with twisted polarization. *Phys. Rev. Res.* **2021**, *3*, 013249.
(34) Gerlach, W.; Stern, O. Der experimentelle nachweis der richtungsquantelung im magnetfeld. *Z. Phys.* **1922**, *9*, 349−352.
(35) Hirsch, J. E. Spin hall effect. *Phys. Rev. Lett.* **1999**, *83*, 1834.
(36) Li, Y.; Bruder, C.; Sun, C. P. Generalized Stern-Gerlach effect for chiral molecules. *Phys. Rev. Lett.* **2007**, *99*, 130403.
(37) Li, X.; Shapiro, M. Theory of the optical spatial separation of racemic mixtures of chiral molecules. *J. Chem. Phys.* **2010**, *132*, 194315.
(38) Chen, Y.-Y.; Ye, C.; Zhang, Q.; Li, Y. Enantio-discrimination via light deflection effect. *J. Chem. Phys.* **2020**, *152*, 204305.
(39) Kane, C. L.; Mele, E. J. Quantum spin Hall effect in graphene. *Phys. Rev. Lett.* **2005**, *95*, 226801.
(40) Thouless, D. J.; Kohmoto, M.; Nightingale, M. P.; den Nijs, M. Quantized Hall conductance in a two-dimensional periodic potential. *Phys. Rev. Lett.* **1982**, *49*, 405.
(41) Hasan, M. Z.; Kane, C. L. Colloquium: topological insulators. *Rev. Mod. Phys.* **2010**, *82*, 3045.
(42) Kolodrubetz, M. H.; Nathan, F.; Gazit, S.; Morimoto, T.; Moore, J. E. Topological floquet-thouless energy pump. *Phys. Rev. Lett.* **2018**, *120*, 150601.
(43) Mondragon-Shem, I.; Martin, I.; Alexandradinata, A.; Cheng, M. Quantized frequency-domain polarization of driven phases of matter. *arXiv* **2018**, 1811.10632.
(44) Nathan, F.; Martin, I.; Refael, G. Topological frequency conversion in a driven dissipative quantum cavity. *Phys. Rev. B* **2019**, *99*, 094311.
(45) Oka, T.; Kitamura, S. Floquet engineering of quantum materials. *Annu. Rev. Condens. Matter Phys.* **2019**, *10*, 387−408.
(46) Leboeuf, P.; Kurchan, J.; Feingold, M.; Arovas, D. P. Phase-space localization: topological aspects of quantum chaos. *Phys. Rev. Lett.* **1990**, *65*, 3076.
(47) Leboeuf, P.; Kurchan, J.; Feingold, M.; Arovas, D. P. Topological aspects of quantum chaos. *Chaos* **1992**, *2*, 125−130.
(48) Martin, I.; Refael, G.; Halperin, B. Topological frequency conversion in strongly driven quantum systems. *Phys. Rev. X* **2017**, *7*, 041008.
(49) Ordonez, A. F.; Smirnova, O. Propensity rules in photoelectron circular dichroism in chiral molecules. II. General picture. *Phys. Rev. A* **2019**, *99*, 043417.
(50) Lehmann, K. K. Influence of spatial degeneracy on rotational spectroscopy: Three-wave mixing and enantiomeric state separation of chiral molecules. *J. Chem. Phys.* **2018**, *149*, 094201.
(51) Leibscher, M.; Giesen, T. F.; Koch, C. P. Principles of enantio-selective excitation in three-wave mixing spectroscopy of chiral molecules. *J. Chem. Phys.* **2019**, *151*, 014302.
(52) Simons, J. *An introduction to theoretical chemistry*; Cambridge University Press: Cambridge, 2003.
(53) Boyers, E.; Crowley, P. J. D.; Chandran, A.; Sushkov, A. O. Exploring 2D Synthetic Quantum Hall Physics with a Quasiperiodically Driven Qubit. *Phys. Rev. Lett.* **2020**, *125*, 160505.
(54) Samoilenko, A. M. *Elements of the mathematical theory of multi-frequency oscillations*; Springer Science & Business Media: Berlin, 2012; Vol. *71*.
(55) Bernevig, B. A.; Zhang, S.-C. Quantum spin Hall effect. *Phys. Rev. Lett.* **2006**, *96*, 106802.
(56) Schellman, J. A. Circular dichroism and optical rotation. *Chem. Rev.* **1975**, *75*, 323−331.
(57) Park, G. B.; Field, R. W. Perspective: The first ten years of broadband chirped pulse Fourier transform microwave spectroscopy. *J. Chem. Phys.* **2016**, *144*, 200901.
(58) Belkin, M.; Kulakov, T.; Ernst, K.-H.; Yan, L.; Shen, Y. Sum-frequency vibrational spectroscopy on chiral liquids: a novel technique to probe molecular chirality. *Phys. Rev. Lett.* **2000**, *85*, 4474.

https://doi.org/10.1021/acs.jpclett.1c04161
J. Phys. Chem. Lett. 2022, 13, 2434−2441

(59) Fischer, P.; Buckingham, A.; Beckwitt, K.; Wiersma, D.; Wise, F. New electro-optic effect: sum-frequency generation from optically active liquids in the presence of a dc electric field. *Phys. Rev. Lett.* **2003**, *91*, 173901.
(60) Faure, F.; Zhilinskii, B. Topological Chern indices in molecular spectra. *Phys. Rev. Lett.* **2000**, *85*, 960.
(61) Schwennicke, K.; Yuen-Zhou, J. Optical activity from the exciton Aharonov−Bohm effect: A Floquet engineering approach. *J. Phys. Chem. C* **2020**, *124*, 4206−4214.
(62) Ordonez, A. F.; Ayuso, D.; Decleva, P.; Smirnova, O. Geometric magnetism and new enantio-sensitive observables in photoionization of chiral molecules. *arXiv* **2021**, 2106.14264.

https://doi.org/10.1021/acs.jpclett.1c04161
J. Phys. Chem. Lett. 2022, 13, 2434−2441

Enantioselective Topological Frequency Conversion

Kai Schwennicke and Joel Yuen-Zhou*

Department of Chemistry and Biochemistry, University of California, San Diego, La Jolla, California 92093, United States

E-mail: joelyuen@ucsd.edu

1 Rotational eigenstates

Here we present the low angular momentum eigenstates of the asymmetric top. For completeness, we reintroduce the asymmetric top Hamiltonian

$$H_0 = AJ_a^2 + BJ_b^2 + CJ_c^2, \tag{1}$$

where J_a, J_b, J_c are the angular momentum operators with respect to the principal axes $\hat{\boldsymbol{a}}$, $\hat{\boldsymbol{b}}$, $\hat{\boldsymbol{c}}$, and $A > B > C$ are the corresponding rotational constants. The $B = C$ case corresponds to a prolate top with eigenstates labeled $|J, K, M\rangle$, where $J = 0, 1, 2...$ is the rotational quantum number and $M, K = -J, -J+1, -J+2, ..., J$ are the quantum numbers that characterize the projection of the total angular momentum along the a-principal axis and z-laboratory-fixed axis. The eigenstates of the asymmetric top Hamiltonian can be

expressed as superpositions of the prolate top eigenstates as follows:

$$|J,\tau,M\rangle = \sum_K A_K^{J,M}(\tau)|J,K,M\rangle. \tag{2}$$

Note that the quantum numbers J, M are conserved by H_0, and τ serves as the quantum number to differentiate between states with the same J and M. The eigenstates of Eq. 1 with a rotational quantum number of $J=0$ or $J=1$ are

$$\begin{aligned}
|0,\tau=1,0\rangle &\equiv |0,K=0,0\rangle,\\
|1,\tau=1,M\rangle &\equiv |1,K=0,M\rangle,\\
|1,\tau=2,M\rangle &\equiv \frac{1}{\sqrt{2}}|1,K=1,M\rangle - \frac{1}{\sqrt{2}}|1,K=-1,M\rangle,\\
|1,\tau=3,M\rangle &\equiv \frac{1}{\sqrt{2}}|1,K=1,M\rangle + \frac{1}{\sqrt{2}}|1,K=-1,M\rangle,
\end{aligned} \tag{3}$$

where $M=-1,0,1$[1]. In the main text, we do not couple the states $|1,\tau=1,M\rangle$ to others, and thus ignore them.

2 Change of Basis

We present the necessary change of basis to obtain the effective Hamiltonian presented in Eq. 8 in the main text. We first introduce $|2,B\rangle = \frac{1}{\sqrt{2}}(|2,1\rangle + |2,-1\rangle)$ and $|2,D\rangle = \frac{1}{\sqrt{2}}(|2,1\rangle - |2,-1\rangle)$, which we refer to as the "bright" and "dark" state respectively. It is easy to see that bright state couples to $|1,0\rangle$ and $|3,0\rangle$, while the dark state is uncoupled (see Eq. 7). Ignoring the dark state, the Hamiltonian in the rotating frame becomes

$$\mathcal{H}^{R,S}(t) = \frac{1}{2}\begin{pmatrix} -2\hbar\delta & -\frac{\mu_b^{R,S}}{\sqrt{3}}\mathcal{E}_{21}(t) & -\frac{i\mu_c^{R,S}}{\sqrt{3}}\mathcal{E}_{31}(t)\\ -\frac{\mu_b^{R,S}}{\sqrt{3}}\mathcal{E}_{21}(t) & 0 & -\frac{\mu_a^{R,S}}{2}\mathcal{E}_{32}(t)\\ \frac{i\mu_c^{R,S}}{\sqrt{3}}\mathcal{E}_{31}(t) & -\frac{\mu_a^{R,S}}{2}\mathcal{E}_{32}(t) & 2\hbar\delta \end{pmatrix} \tag{4}$$

In the complex basis $|+\Pi\rangle, |0\rangle, |-\Pi\rangle$, where $|\pm\Pi\rangle = \frac{1}{\sqrt{2}}(|1,0\rangle \pm i|3,0\rangle)$ and $|0\rangle = |2,B\rangle$, Eq. 4 becomes

$$\begin{aligned}\mathcal{H}^{R,S}(t) = &-\frac{\mu_b^{R,S}\mathcal{E}_{21}(t)}{2\sqrt{3}\hbar}L_x - \frac{\mu_a^{R,S}\mathcal{E}_{32}(t)}{4\hbar}L_y \\ &+ \frac{\mu_c^{R,S}\mathcal{E}_{31}(t)}{2\sqrt{3}\hbar}L_z - \frac{\delta}{2\hbar}(L_+^2 + L_-^2)\end{aligned} \tag{5}$$

where $L_x = \frac{\hbar}{\sqrt{2}}\begin{pmatrix}0&1&0\\1&0&1\\0&1&0\end{pmatrix}$, $L_y = \frac{\hbar}{\sqrt{2}}\begin{pmatrix}0&-i&0\\i&0&-i\\0&i&0\end{pmatrix}$, $L_z = \hbar\begin{pmatrix}1&0&0\\0&0&0\\0&0&-1\end{pmatrix}$ are the angular momentum operators for a spin-1 particle and $L_+ = \hbar\sqrt{2}\begin{pmatrix}0&1&0\\0&0&1\\0&0&0\end{pmatrix}$, $L_-= \hbar\sqrt{2}\begin{pmatrix}0&0&0\\1&0&0\\0&1&0\end{pmatrix}$ are the corresponding ladder operators. Eq. 5 is the effective Hamiltonian used to study the topology of the system presented in the main text.

3 Adiabatic perturbation theory

For completeness, we briefly review adiabatic perturbation theory. Let $|\tilde{\psi}(t)\rangle = \sum_l \tilde{c}_l(t)|\epsilon_l(t)\rangle$ be the solution of the time-dependent Schrödinger equation (TDSE) $i\hbar\partial_t|\tilde{\psi}(t)\rangle = \mathcal{H}(t)|\tilde{\psi}(t)\rangle$, where $\{|\epsilon_l(t)\rangle\}$ are the adiabatic eigenstates satisfying $\mathcal{H}(t)|\epsilon_l(t)\rangle = \epsilon_l(t)|\epsilon_l(t)\rangle$. Employing the TDSE, the following differential equation is obtained for $\tilde{c}_l(t)$,

$$i\hbar\partial_t\tilde{c}_l(t) = \epsilon_l(t)\tilde{c}_l(t) - i\hbar\sum_{l'}\langle\epsilon_l(t)|\boldsymbol{\omega}\cdot\nabla_{\boldsymbol{\omega}t}|\epsilon_{l'}(t)\rangle\tilde{c}_{l'}(t), \tag{6}$$

where $\boldsymbol{\omega} = (\omega_1, \omega_2)$. Ignoring non-adiabatic terms in Eq. 6 for $l' \neq l$,

$$\tilde{c}_l(t) \approx \tilde{c}_l(0)e^{-i\int_0^t dt'[\epsilon_l(t') - i\hbar\langle\epsilon_l(t')|\boldsymbol{\omega}\cdot\nabla_{\boldsymbol{\omega}t}|\epsilon_l(t')\rangle]/\hbar}. \tag{7}$$

Hereafter, we assume that the system is initialized in the $l-$th adiabatic state $|\tilde{\psi}(0)\rangle = |\epsilon_l(0)\rangle$. Eq. 7 is a statement of the adiabatic theorem and implies that the system shall remain in the $l-$th adiabatic state, $|\tilde{\psi}(t)\rangle \approx (\text{phase factor}) \times |\epsilon_l(t)\rangle$.

However, we are interested in $O(\hbar\omega)$ non-adiabatic corrections to Eq. 7. We rewrite $\tilde{c}_{l'} = \hbar\boldsymbol{\omega}\tilde{c}_l(t)a_{l'}(t)$ for $l' \neq l$,

$$|\tilde{\psi}(t)\rangle = \tilde{c}_l(t)[|\epsilon_l(t)\rangle + \sum_{l'\neq l} \hbar\boldsymbol{\omega} a_{l'}(t)|\epsilon_{l'}(t)\rangle], \tag{8}$$

and insert this ansatz into Eq. 6,

$$\epsilon_l(t)\tilde{c}_l(t)a_{l'}(t)\hbar\boldsymbol{\omega} + O(\hbar^2\boldsymbol{\omega}^2) = \hbar\boldsymbol{\omega}\epsilon_{l'}(t)\tilde{c}_l(t)a_{l'}(t) - i\hbar\langle\epsilon_{l'}(t)|\boldsymbol{\omega}\cdot\nabla_{\boldsymbol{\omega}t}|\epsilon_l(t)\rangle\tilde{c}_l(t) + O(\hbar^2\boldsymbol{\omega}^2), \tag{9}$$

where we used $\partial_t a_{l'}(t) = \hbar\boldsymbol{\omega}\cdot\nabla_{\omega t}a_{l'}(t)$. Solving for $a_{l'}(t)$, the $O(\hbar\omega)$ wavefunction is,

$$|\tilde{\psi}(t)\rangle = \tilde{c}_l(t)\left[|\epsilon_l(t)\rangle - i\hbar\sum_{l'\neq l}\frac{|\epsilon_{l'}(t)\rangle\langle\epsilon_{l'}(t)|\boldsymbol{\omega}\cdot\nabla_{\boldsymbol{\omega}t}|\epsilon_l(t)\rangle}{\epsilon_l(t)-\epsilon_{l'}(t)}\right]. \tag{10}$$

Calculating $\mathcal{P}_{av}(\omega_1)$ and $\mathcal{P}_{av}(\omega_2)$

Here, $\langle\tilde{\psi}(t)|\partial_{\omega_i t}\mathcal{H}(t)|\tilde{\psi}(t)\rangle$ and $P_{av}(\omega_i)$ are derived when the system is initiated in the adiabatic state $|\epsilon_l(0)\rangle$ and evolved near the adiabatic limit. Employing Eq. 10 for $|\tilde{\psi}(t)\rangle$, and making the change of variables $(\omega_1 t, \omega_2 t) = (\theta_1, \theta_2)$, the following expression to $O(\hbar\omega)$ is obtained:

$$\begin{aligned}
\langle\tilde{\psi}(t)|\nabla_{\boldsymbol{\omega}t}\mathcal{H}(t)|\tilde{\psi}(t)\rangle &= \langle\epsilon_l(\boldsymbol{\theta})|\nabla_{\boldsymbol{\theta}}\mathcal{H}(\boldsymbol{\theta})|\epsilon_l(\boldsymbol{\theta})\rangle - \left\{i\hbar\sum_{l'\neq l}\frac{\langle\epsilon_l(\boldsymbol{\theta})|\nabla_{\boldsymbol{\theta}}\mathcal{H}(\boldsymbol{\theta})|\epsilon_{l'}(\boldsymbol{\theta})\rangle\langle\epsilon_{l'}(\boldsymbol{\theta})|\boldsymbol{\omega}\cdot\nabla_{\boldsymbol{\theta}}|\epsilon_l(\boldsymbol{\theta})\rangle}{\epsilon_l(\boldsymbol{\theta})-\epsilon_{l'}(\boldsymbol{\theta})} + \text{h.c}\right\} \\
&= \nabla_{\boldsymbol{\theta}}\epsilon_l(\boldsymbol{\theta}) - \left\{i\hbar\langle\nabla_{\boldsymbol{\theta}}\epsilon_l(\boldsymbol{\theta})|\boldsymbol{\omega}\cdot\nabla_{\boldsymbol{\theta}}|\epsilon_l(\boldsymbol{\theta})\rangle + \text{h.c}]\right\} \\
&= \nabla_{\boldsymbol{\theta}}\epsilon_l(\boldsymbol{\theta}) - \hbar\boldsymbol{\omega}\times\hat{\boldsymbol{v}}_\perp F_l(\boldsymbol{\theta}),
\end{aligned} \tag{11}$$

where $\boldsymbol{\omega}\times\hat{\boldsymbol{v}}_\perp = (\omega_2, -\omega_1)$ and $F_l(\boldsymbol{\theta}) = i\langle\partial_{\theta_1}\epsilon_l(\boldsymbol{\theta})|\partial_{\theta_2}\epsilon_l(\boldsymbol{\theta})\rangle + \text{h.c.}$ is the Berry curvature of

the $l-$th band.

4 Analytical evaluation of Chern numbers

Here, we analytically compute the Chern numbers for the bands of the system in the main text when $\delta = 0$. We follow the procedure described in[2]. We first consider the three-level Hamiltonian:

$$\mathcal{H}(\boldsymbol{\theta}) = \sum_{s=\pm 1} s h_3(\boldsymbol{\theta}) |s\rangle\langle s| + \Big\{ [h_1(\boldsymbol{\theta}) - i s h_2(\boldsymbol{\theta})] |s\rangle\langle 0| + \text{h.c.} \Big\}, \tag{12}$$

where $h_1(\boldsymbol{\theta})$, $h_2(\boldsymbol{\theta})$, $h_3(\boldsymbol{\theta})$ are real valued. Next, we invoke the unitary transformation $U(\boldsymbol{\theta}) = \sum_{s=0,\pm 1} e^{is\alpha(\boldsymbol{\theta})} |s\rangle\langle s|$, such that $\tan\alpha(\boldsymbol{\theta}) = h_2(\boldsymbol{\theta})/h_1(\boldsymbol{\theta})$, to define the real valued Hamiltonian,

$$\begin{aligned} \mathcal{H}'(\boldsymbol{\theta}) &= U(\boldsymbol{\theta}) \mathcal{H}(\boldsymbol{\theta}) U^\dagger(\boldsymbol{\theta}) \\ &= \sum_{s=\pm 1} s h_3(\boldsymbol{\theta}) |s\rangle\langle s| + \sqrt{h_1^2(\boldsymbol{\theta}) + h_2^2(\boldsymbol{\theta})} (|s\rangle\langle 0| + \text{h.c.}). \end{aligned} \tag{13}$$

A set of eigenstates for $\mathcal{H}'(\boldsymbol{\theta})$ can be defined as $|\epsilon'_l(\boldsymbol{\theta})\rangle = \sum_{s=0,\pm 1} c_{l,s}(\boldsymbol{\theta}) |s\rangle$, where the coefficients $c_{l,s}(\boldsymbol{\theta})$ are real. The eigenstates of $\mathcal{H}(\boldsymbol{\theta})$ are

$$|\epsilon_l(\boldsymbol{\theta})\rangle = U^\dagger(\boldsymbol{\theta}) |\epsilon'_l(\boldsymbol{\theta})\rangle = \sum_{s=0,\pm 1} c_{l,s}(\boldsymbol{\theta}) e^{-is\alpha(\boldsymbol{\theta})} |s\rangle. \tag{14}$$

The Berry connection for the $l-$th band is

$$\begin{aligned} \boldsymbol{A}_l(\boldsymbol{\theta}) &= i \langle \epsilon_l(\boldsymbol{\theta}) | \nabla_{\boldsymbol{\theta}} | \epsilon_l(\boldsymbol{\theta}) \rangle \\ &= \nabla_{\boldsymbol{\theta}} \alpha(\boldsymbol{\theta}) \sum_{s=\pm 1} s c_{l,s}^2(\boldsymbol{\theta}), \end{aligned} \tag{15}$$

where we used the fact that $\sum_{s=0,\pm1} c_{l,s}(\boldsymbol{\theta})\nabla_{\boldsymbol{\theta}} c_{l,s}(\boldsymbol{\theta}) = \frac{1}{2}\nabla_{\boldsymbol{\theta}} \sum_{s=0,\pm1} |c_{l,s}|^2 = 0$. The Berry curvature is defined as the z-component of the curl of the Berry connection, *i.e.*, $F_l(\boldsymbol{\theta}) = (\nabla_{\boldsymbol{\theta}} \times \boldsymbol{A}_l(\boldsymbol{\theta})) \cdot \hat{z}$. Note that there are singularities in the Berry connection when $\nabla_{\boldsymbol{\theta}}\alpha(\boldsymbol{\theta}) = \frac{h_1(\boldsymbol{\theta})\nabla_{\boldsymbol{\theta}} h_2(\boldsymbol{\theta}) - h_2(\boldsymbol{\theta})\nabla_{\boldsymbol{\theta}} h_1(\boldsymbol{\theta})}{h_1^2(\boldsymbol{\theta}) + h_2^2(\boldsymbol{\theta})}$ is undefined; they occur at the critical points where $h_1(\boldsymbol{\theta}) = h_2(\boldsymbol{\theta}) = 0$.

Considering Eqs. 8 and 9 from the main text and taking $\delta = 0$, the values $h_1^{R,S}(\boldsymbol{\theta})$, $h_2^{R,S}(\boldsymbol{\theta})$, $h_3^{R,S}(\boldsymbol{\theta})$ are

$$
\begin{aligned}
h_1^{R,S}(\boldsymbol{\theta}) &= -\frac{\mu_b^{R,S} E_{21} \sin(\theta_1)}{2\sqrt{6}}, \\
h_2^{R,S}(\boldsymbol{\theta}) &= -\frac{\mu_a^{R,S} E_{32} \sin(\theta_2)}{4\sqrt{2}}, \\
h_3^{R,S}(\boldsymbol{\theta}) &= \frac{\mu_c^{R,S}}{2\sqrt{3}} E_{31}[m - \cos(\theta_1) - \cos(\theta_2)],
\end{aligned}
\tag{16}
$$

and the aforementioned singularities occur at the $\boldsymbol{\theta} = (\theta_1, \theta_2)$ values $\boldsymbol{\theta}_{00} = (0,0)$, $\boldsymbol{\theta}_{0\pi} = (0,\pi)$, $\boldsymbol{\theta}_{\pi 0} = (\pi, 0)$, and $\boldsymbol{\theta}_{\pi\pi} = (\pi,\pi)$. Physically, these critical points indicate geometric conditions where certain components of light-matter coupling vanish.

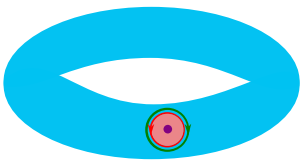

Figure 1: *Contour integration procedure to evaluate Chern number* $C_l^{R,S}$. The closed curve ∂_r bounds both the pink region, which contains the singularity of $\boldsymbol{A}_l^{R,S}(\boldsymbol{\theta})$, and the blue region, which is rest of the torus. To apply Stokes theorem, we integrate counter-clockwise (red curve) along ∂_r to find the surface integral for the pink region, and clockwise along ∂_R (green curve) to find the surface integral for the blue region. The procedure can be extended to an arbitrary number of singularities of $\boldsymbol{A}_l^{R,S}(\boldsymbol{\theta})$.

The Chern number for the $R-$ and $S-$ enantiomer is proportional to the surface integral

of the corresponding Berry curvature over the torus $\mathbb{T}$,

$$C_l^{R,S} = \frac{1}{2\pi} \int_{\mathbb{T}} d\boldsymbol{\theta} F_l^{R,S}(\boldsymbol{\theta}). \tag{17}$$

Using Stokes theorem, it can be written as a contour integral of the Berry connection; however, the singularities must be removed. To motivate the general procedure, first consider the case where the Berry connection $\boldsymbol{A}_l^{R,S}(\boldsymbol{\theta})$ contains only one singularity. The curve ∂_r can be drawn, such that it defines an infinitesimal region containing the singularity (region I) and the rest of the torus (region II) (see Fig. 1). Applying a gauge transformation $|\epsilon_l^{R,S}(\boldsymbol{\theta})\rangle \to e^{i\phi_l^{R,S}(\boldsymbol{\theta})}|\epsilon_l^{R,S}(\boldsymbol{\theta})\rangle$ in region I can remove the singularity, $\boldsymbol{A}_l^{R,S}(\boldsymbol{\theta}) \to \boldsymbol{A}_l'^{R,S}(\boldsymbol{\theta}) = \boldsymbol{A}_l^{R,S}(\boldsymbol{\theta}) - \nabla_{\boldsymbol{\theta}}\phi_l^{R,S}(\boldsymbol{\theta})$, while the Berry curvature is unaffected [2,3]. Taking $\nabla_{\boldsymbol{\theta}}\phi_l^{R,S}(\boldsymbol{\theta}) = \boldsymbol{A}_l^{R,S}(\boldsymbol{\theta})$ achieves this desired result. The Chern numbers can then be written as the summation of contour integrals for each region:

$$\begin{aligned}
C_l^{R,S} &= \frac{1}{2\pi} \int_{\mathbb{T}} d\boldsymbol{\theta} F_l^{R,S}(\boldsymbol{\theta}) \\
&= \frac{1}{2\pi} \oint_{\partial_r} d\boldsymbol{\theta} \cdot \boldsymbol{A}_l'^{R,S}(\boldsymbol{\theta}) - \frac{1}{2\pi} \oint_{\partial_R} d\boldsymbol{\theta} \cdot \boldsymbol{A}_l^{R,S}(\boldsymbol{\theta}) \\
&= \frac{1}{2\pi} \oint_{\partial_r} d\boldsymbol{\theta} \cdot [\boldsymbol{A}^{R,S}{}_l(\boldsymbol{\theta}) - \nabla_{\boldsymbol{\theta}}\phi_l^{R,S}(\boldsymbol{\theta})] - \frac{1}{2\pi} \oint_{\partial_R} d\boldsymbol{\theta} \cdot \boldsymbol{A}_l^{R,S}(\boldsymbol{\theta}) \\
&= -\frac{1}{2\pi} \oint_{\partial_r} d\boldsymbol{\theta} \cdot \nabla_{\boldsymbol{\theta}}\phi_l^{R,S}(\boldsymbol{\theta}) \\
&= -\frac{1}{2\pi} \oint_{\partial_r} d\boldsymbol{\theta} \cdot \boldsymbol{A}_l^{R,S}(\boldsymbol{\theta}).
\end{aligned} \tag{18}$$

In going from the first to the second line, we applied Stokes theorem in region I by traversing ∂_r in a counterclockwise fashion, and in region II by doing so in a clockwise way (see Fig. 1).

If the Berry connection $\boldsymbol{A}_l^{R,S}(\boldsymbol{\theta})$ contains multiple singularities $\boldsymbol{\theta}_{ij}$, then local gauge transformations must be carried out in multiple regions to remove all of them. Then the

Chern number results in

$$C_l^{R,S} = -\sum_{ij} \frac{1}{2\pi} \oint_{\partial_{r_{ij}}} d\boldsymbol{\theta} \cdot \boldsymbol{A}_l^{R,S}(\boldsymbol{\theta}) \tag{19}$$

where the curves $\{\partial_{r_{ij}}\}$ enclose an infinitesimal region around each of the singularities $\boldsymbol{\theta}_{ij}$. Therefore, the Chern number can be calculated by studying the behavior of $\boldsymbol{A}_l^{R,S}(\boldsymbol{\theta})$ near the singularities.

Let $\boldsymbol{q} = (q_1, q_2)$ be a small displacement from the point $\boldsymbol{\theta}_{ij}$. Since $\sin(x) \approx x$ and $\sin(\pi + x) \approx -x$ as $x \to 0$, then

$$\begin{aligned}
\alpha^{R,S}(\boldsymbol{\theta}_{00} + \boldsymbol{q}) &\approx \beta^{R,S}, \\
\alpha^{R,S}(\boldsymbol{\theta}_{0\pi} + \boldsymbol{q}) &\approx -\beta^{R,S}, \\
\alpha^{R,S}(\boldsymbol{\theta}_{\pi 0} + \boldsymbol{q}) &\approx -\beta^{R,S}, \\
\alpha^{R,S}(\boldsymbol{\theta}_{\pi\pi} + \boldsymbol{q}) &\approx \beta^{R,S},
\end{aligned} \tag{20}$$

where $\tan\beta^{R,S} = \frac{\sqrt{3}\mu_a^{R,S} E_{32} q_2}{2\mu_b^{R,S} E_{21} q_1}$. The gradients $\nabla_{\boldsymbol{q}} \alpha^{R,S}(\boldsymbol{\theta})$ near the critical points can be readily evaluated in polar coordinates, $|\boldsymbol{q}|e^{i\gamma} = q_1 + iq_2$,

$$\begin{aligned}
\nabla_{\boldsymbol{q}} \alpha^{R,S}(\boldsymbol{\theta}_{00} + \boldsymbol{q}) &= -\nabla_{\boldsymbol{q}} \alpha^{R,S}(\boldsymbol{\theta}_{\pi 0} + \boldsymbol{q}) \\
&= -\nabla_{\boldsymbol{q}} \alpha^{R,S}(\boldsymbol{\theta}_{0\pi} + \boldsymbol{q}) \\
&= \nabla_{\boldsymbol{q}} \alpha^{R,S}(\boldsymbol{\theta}_{\pi\pi} + \boldsymbol{q}) \\
&\approx \frac{1}{|\boldsymbol{q}|} \frac{(\sqrt{3}\mu_a^{R,S} E_{32})(2\mu_b^{R,S} E_{21})}{(\sqrt{3}\mu_a^{R,S} E_{32})^2 \sin^2\gamma + (2\mu_b^{R,S} E_{21})^2 \cos^2\gamma} \hat{\boldsymbol{\gamma}}.
\end{aligned} \tag{21}$$

The line integral of $\nabla_{\boldsymbol{q}} \alpha^{R,S}(\boldsymbol{\theta}_{00} + \boldsymbol{q})$ over a small circle in the limit when $|\boldsymbol{q}| \to 0$,

$$
\begin{aligned}
&\oint_{|\boldsymbol{q}|\to 0} d\boldsymbol{q}\cdot\nabla_{\boldsymbol{q}}\alpha^{R,S}(\boldsymbol{\theta}_{00}+\boldsymbol{q}) \\
=&\Big(\int_0^{\pi/2^-} d\gamma+\int_{\pi/2^+}^{3\pi/2^-} d\gamma \\
&+\int_{3\pi/2^+}^{2\pi} d\gamma\Big)\frac{(\sqrt{3}\mu_a^{R,S}E_{32})(2\mu E_{21})}{(\sqrt{3}\mu_a^{R,S}E_{32})^2\sin^2\gamma+(2\mu_b^{R,S}E_{21})^2\cos^2\gamma} \\
=&\Big(\int_0^{\mathrm{sgn}[(\mu_a^{R,S}E_{32})(\mu_b^{R,S}E_{21})]\infty} dx+\int_{-\mathrm{sgn}[(\mu_a^{R,S}E_{32})(\mu_b^{R,S}E_{21})]\infty}^{\mathrm{sgn}[(\mu_a^{R,S}E_{32})(\mu_b^{R,S}E_{21})]\infty} dx \\
&+\int_{-\mathrm{sgn}[(\mu_a^{R,S}E_{32})(\mu_b^{R,S}E_{21})]\infty}^{0} dx\Big)\frac{1}{1+x^2} \\
=&2\pi\mathrm{sgn}[(\mu_a^{R,S}E_{32})(\mu_b^{R,S}E_{21})].
\end{aligned}
\tag{22}
$$

In the second line, we split the integral into three parts, noticing that the integral in the remaining infinitesimal regions around $\gamma=\pi/2$ and $\gamma=3\pi/2$ vanish given that the integrand is finite, $\int_{\pi/2^-}^{\pi/2^+} d\gamma(\cdot)=\int_{3\pi/2^-}^{3\pi/2^+} d\gamma(\cdot)=0$. In the third line, we let $x=\frac{\sqrt{3}\mu_a^{R,S}E_{32}}{2\mu_b^{R,S}E_{21}}\tan\gamma$, and $dx=\frac{\sqrt{3}\mu_a^{R,S}E_{32}}{\mu_b^{R,S}E_{21}}\sec^2\gamma d\gamma$ and recognized that $x\to\mathrm{sgn}[(\mu_a^{R,S}E_{32})(\mu_b^{R,S}E_{21})]\infty$ as $\gamma\to(\pi/2)^-,(3\pi/2)^-$ and $x\to-\mathrm{sgn}[(\mu_a^{R,S}E_{32})(\mu_b^{R,S}E_{21})]\infty$ as $\gamma\to(\pi/2)^+,(3\pi/2)^+$.

The procedure of Eqs. (21) and (22) can be repeated for the other critical points, yielding,

$$
\begin{aligned}
\oint_{|\boldsymbol{q}|\to 0} d\boldsymbol{q}\nabla_{\boldsymbol{q}}\alpha^{R,S}(\boldsymbol{\theta}_{0\pi}+\boldsymbol{q})&=-2\pi\mathrm{sgn}[(\mu_a^{R,S}E_{32})(\mu_b^{R,S}E_{21})], \\
\oint_{|\boldsymbol{q}|\to 0} d\boldsymbol{q}\nabla_{\boldsymbol{q}}\alpha^{R,S}(\boldsymbol{\theta}_{\pi 0}+\boldsymbol{q})&=-2\pi\mathrm{sgn}[(\mu_a^{R,S}E_{32})(\mu_b^{R,S}E_{21})], \\
\oint_{|\boldsymbol{q}|\to 0} d\boldsymbol{q}\nabla_{\boldsymbol{q}}\alpha^{R,S}(\boldsymbol{\theta}_{\pi\pi}+\boldsymbol{q})&=2\pi\mathrm{sgn}[(\mu_a^{R,S}E_{32})(\mu_b^{R,S}E_{21})].
\end{aligned}
\tag{23}
$$

Using Eqs. 15 and 19, the Chern number for the l-th band is

$$C_l^{R,S} = -\sum_{ij} \frac{1}{2\pi} \oint_{\partial_{r_{ij}}} d\boldsymbol{\theta} \cdot \boldsymbol{A}_l^{R,S}(\boldsymbol{\theta})$$
$$= -\text{sgn}[(\mu_a^{R,S} E_{21})(\mu_b^{R,S} E_{32})] \sum_{s=\pm 1} s[|c_{l,s}^{R,S}(\boldsymbol{\theta}_{00})|^2 - |c_{l,s}^{R,S}(\boldsymbol{\theta}_{0\pi})|^2 - |c_{l,s}^{R,S}(\boldsymbol{\theta}_{\pi 0})|^2 + |c_{l,s}^{R,S}(\boldsymbol{\theta}_{\pi\pi})|^2] \tag{24}$$

For $|m| < 2$ the Chern numbers for the upper, middle, and lower adiabatic states can be seen to yield,

$$\begin{aligned} C_U^{R,S} &= 2\text{sgn}[m(\mu_a^{R,S} E_{32})(\mu_b^{R,S} E_{21})(\mu_c^{R,S} E_{31})], \\ C_M^{R,S} &= 0, \\ C_L^{R,S} &= -2\text{sgn}[m(\mu_a^{R,S} E_{32})(\mu_b^{R,S} E_{21})(\mu_c^{R,S} E_{31})]. \end{aligned} \tag{25}$$

For $|m| > 2$, all $C_l^{R,S} = 0$. For the benefit of the reader, Table 1 provides an example calculation of the upper band Chern number $C_U^{R,S}$ for $|m| < 2$

Table 1: *Example Chern number calculation.* Shown are the values of the $|s = \pm 1\rangle$ amplitudes $|c_{U,s}^{R,S}(\boldsymbol{\theta}_{00})|^2$ for the upper band eigenstate at the singularity points $\boldsymbol{\theta}_{ij}$ for $|m| < 2$. Using these values and Eq. 24, we find that $C_U^{R,S} = 2\text{sgn}[m(\mu_a^{R,S} E_{32})(\mu_b^{R,S} E_{21})(\mu_c^{R,S} E_{31})]$.

	$\lvert c_{U,s}^{R,S}(\boldsymbol{\theta}_{00})\rvert^2$	$\lvert c_{U,s}^{R,S}(\boldsymbol{\theta}_{0\pi})\rvert^2$	$\lvert c_{U,s}^{R,S}(\boldsymbol{\theta}_{\pi 0})\rvert^2$	$\lvert c_{U,s}^{R,S}(\boldsymbol{\theta}_{\pi\pi})\rvert^2$
$s = 1$	$\frac{1}{2} - \frac{1}{2}\text{sgn}[(\mu_c^{R,S} E_{31})]$	$\frac{1}{2} + \frac{1}{2}\text{sgn}[m(\mu_c^{R,S} E_{31})]$	$\frac{1}{2} + \frac{1}{2}\text{sgn}[m(\mu_c^{R,S} E_{31})]$	$\frac{1}{2} + \frac{1}{2}\text{sgn}[(\mu_c^{R,S} E_{31})]$
$s = -1$	$\frac{1}{2} + \frac{1}{2}\text{sgn}[(\mu_c^{R,S} E_{31})]$	$\frac{1}{2} - \frac{1}{2}\text{sgn}[m(\mu_c^{R,S} E_{31})]$	$\frac{1}{2} - \frac{1}{2}\text{sgn}[m(\mu_c^{R,S} E_{31})]$	$\frac{1}{2} - \frac{1}{2}\text{sgn}[(\mu_c^{R,S} E_{31})]$

5 Laser shot-noise

The laser shot noise is defined as the width of the photon distribution of the driving field. In the main text the laser field strength is assumed to be approximately $E = 10^{-9}$ a.u., or

$500\,\frac{\mathrm{V}}{\mathrm{m}}$. Assuming that the laser-beam waist area is $A = 1\mathrm{cm}^2$, its power is given by,

$$\begin{aligned} P &= \frac{cA\epsilon_0 E^2}{8\pi} \\ &= \frac{3\times 10^8\,\frac{\mathrm{m}}{\mathrm{s}} \times 1\,\mathrm{cm}^2 \times \frac{1\mathrm{m}^2}{100^2\mathrm{cm}^2} \times 8.85\times 10^{-12}\,\frac{\mathrm{C}^2}{\mathrm{J}\cdot\mathrm{m}} \times (500\frac{\mathrm{V}}{\mathrm{m}})^2}{8\pi} \\ &= 3\,\mathrm{mW} \end{aligned} \tag{26}$$

where c is the speed of light and ϵ_0 is the permittivity of free space. The frequencies of the molecular transitions in the main text are on the order of $v = 10\,\mathrm{GHz}$. Then the expected number of photons produced by the laser after a long enough time $t^* = 2000 \times 2\pi/\omega_2$ which guarantees TFC is

$$N = \frac{Pt^*}{hv} = \frac{3\times 10^{-3}\mathrm{W} \times 8\times 10^{-3}\mathrm{s}}{6.63\times 10^{-34}\mathrm{J}\cdot\mathrm{s} \times 10\times 10^9\mathrm{s}^{-1}} = 4\times 10^{18} \tag{27}$$

The photon distribution is taken to be Poissonian. The standard deviation of this distribution is $\sqrt{N}$, so the laser shot noise is $\sqrt{N} \sim 10^9$.

References

(1) Simons, J. *An introduction to theoretical chemistry*; Cambridge University Press: Cambridge, 2003.

(2) Andrijauskas, T.; Anisimovas, E.; Račiūnas, M.; Mekys, A.; Kudriašov, V.; Spielman, I. B.; Juzeliūnas, G. Three-level Haldane-like model on a dice optical lattice. *Phys. Rev. A* **2015**, *92*, 033617.

(3) Goldman, N.; Anisimovas, E.; Gerbier, F.; Öhberg, P.; Spielman, I. B.; Juzeliūnas, G. Measuring topology in a laser-coupled honeycomb lattice: from Chern insulators to topological semi-metals. *New J. Phys.* **2013**, *15*, 013025.